RSC Advances

PAPER

View Article Online
View Journal | View Issue

Cite this: *RSC Adv.*, 2021, **11**, 946

Electronic phase-crossover and room temperature ferromagnetism in a two-dimensional (2D) spin lattice†

A. K. Nair and S. J. Ray *

Received 16th November 2020
Accepted 26th November 2020

DOI: 10.1039/d0ra09726h

rsc.li/rsc-advances

Tuning of system properties such as electronic and magnetic behaviour through various engineering techniques is necessary for optoelectronic and spintronic applications. In our current work, we employ first-principles methodologies along with Monte-Carlo simulations to comprehensively study the electronic and magnetic behaviour of 2-dimensional (2D) $Cr_2Ge_2Te_6$ (T_c = 61 K), uncovering the impact of strain and electric field on the material. In the presence of strain, we were able to achieve high temperature magnetic ordering in the layer along with observable phase crossover in the electronic state of the system, where the system exhibited transference from semiconducting to half-metallic state. Finally, on coupling strain and electric field remarkable increase in Curie temperature (T_c) ~ 331 K (above 5-fold enhancement from pristine configuration) was observed, which is very well above room temperature. Our inferences have shed light on a relatively new type of coupling method involving strain and electric field which may have tremendous implications in the development of 2D spintronic architecture.

I Introduction

The emergence of two-dimensional (2D) materials has paved the way for the development of several nanoelectronic and spintronic devices.[1] Extensive studies were conducted to explore the electronic properties of these materials which is tunable through the presence of doping,[2,3] strain,[4–6] vacancy[7–9] and electric field[5,10,11] *etc.* In addition, van der Waals heterostructure of these 2D materials can be employed to generate engineered properties for desired applications.[12] The presence of spontaneous magnetism in 2D materials could effectively pave its way in spintronics,[13] which was however limited to the observation of edge-magnetism or vacancy/doping induced magnetism,[14] localised in nature. To establish a long range magnetic ordering (LRMO) in two-dimension, anisotropy is required to establish an energy gap in the spin wave spectrum, overcoming the thermally induced magnon excitation, as theoretically predicted through Onsager's model[15] and Mermin–Wagner–Hohenberg theorem.[16,17] However, the experimental discovery of intrinsic magnetism was recently made in several 2D nanocrystals[18–20] with critical temperature (T_c) below 100 K.

The technological operation of a spintronic device favours ferromagnetic materials with room-temperature magnetic ordering[21] and several of the 2D magnetic materials do not fit the criterion in terms of either being intrinsically antiferromagnetic or not processing a high ordering temperature. However, the magnetic properties can be fine-tuned, as desired, through the application of a few engineering techniques.[22,23] $Cr_2Ge_2Te_6$ (CGT) is a newly discovered 2D magnetic material which has gained great attention recently because of its ability to be exfoliated to the monolayer limit[24] similar to that of CrI_3.[25] Moreover, recent investigations have shown the feasibility of formation of stable heterostructures with several other 2D materials like graphene,[26] CrI_3 [27] and topological insulators,[28,29] observation of photoluminescence[30] and magneto-optical effects.[31] However, the experimental T_c ~ 61 K[20,32] of CGT is well-below room temperature, which is too low for practical spintronics applications. The T_c changes with the change of layer thickness between 40 K to 68 K.[32] In this work, we have explored the possibility of using non-invasive external stimuli like strain and electric field to fine-tune the electronic and magnetic behaviour and change the T_c. Through extensive first-principles based calculations and Monte Carlo (MC) simulations, we have investigated the electronic and magnetic properties of CGT under different strain and electric field conditions. We are able to observe high temperature ferromagnetism (FM) sustaining upto a temperature as high as ~312 K and interesting phase transitions at different parts of the phase diagram. The combination of strain and electric field is a noteworthy mechanism to tune the system properties, which is an unexplored method to the best of our knowledge.

Department of Physics, Indian Institute of Technology Patna, Bihta 801106, India. E-mail: ray@iitp.ac.in; ray.sjr@gmail.com

† Electronic supplementary information (ESI) available. See DOI: 10.1039/d0ra09726h

II Methodology

First-principles based density functional theory (DFT) calculations were used to investigate the electronic structure and magnetic properties of CGT.[33,34] The present methodology involved spin-polarised generalised gradient approximation (SGGA) of the Perdew–Burke–Ernzerhof[35] (PBE) exchange correlation functional. Maximum energy cutoff limit for numerical accuracy was achieved with 150 Ry along with a Monkhorst–Pack[36] k-grid of $9 \times 9 \times 1$ in the reciprocal space for the Brillouin zone. The wave-functions were expanded within a double-ζ polarised basis set under periodic boundary conditions for strain based calculations and Neumann boundary conditions were implemented in the case of electric field applied along the z-direction. In order to account for the on-site Coulomb interaction (U) between the 3d electrons of the Cr-ion, $U = 4$ eV was taken into account. The van der Waal's interaction was incorporated *via* semi-empirical corrections by Grimme D2 and D3 [37] within the GGA.

CGT belongs to space group 162 ($P\bar{3}1m$) having a hexagonal lattice structure with optimised lattice constants of $a_0 = b_0 = 6.8275$ Å. These values were obtained by geometry optimisation with a numerical convergence criterion set with a tolerance of 10^{-6} eV in energy and 10^{-3} eV Å^{-1} in force per atom. A $2 \times 2 \times 1$ supercell of the central structure was prepared for calculations of electronic and magnetic properties. A vacuum space of 20 Å was constructed in the z-direction to eliminate the interaction between the mirror layers. Each Cr atom is surrounded by six neighbouring Te atoms, while each Ge atom is bonded to nearby three Te atoms as shown in Fig. 1. In the present exercise, the electronic and magnetic properties of the system was studied under the influence of biaxial strain. Externally applied strain along a specific direction is defined by, $S = (b - b_0)/b_0$, where $b(b_0)$ is the lattice constant in strained (unstrained) condition. Here we applied biaxial strain (S_b) on the $2 \times 2 \times 1$ supercell of CGT over a range of -8 to 20%. The electric field was applied along the z-direction (E_z), by placing the material between two electrodes and applying equal but opposite voltages (V_z) to them. Statistical Monte Carlo (MC) simulation was used to conduct analysis of the magnetic behaviour of the system considering the 2D Ising model[38] of the hexagonal lattice of CGT. The MC simulation was performed on a 100×100 supercell of CGT with 10^5 iterations and 10^5 MC equilibration sweeps. On the basis of the above information, studies were performed as a function of various strain and electric field cases which are explained later.

III Results and discussion

A Electronic properties

First, we looked at the variation of the electronic structure of CGT as a function of strain and electric field as shown in Fig. 2. Unstrained CGT exhibits a semiconducting character with a direct bandgap of 0.28 eV for both spin-↑ and spin-↓ states,

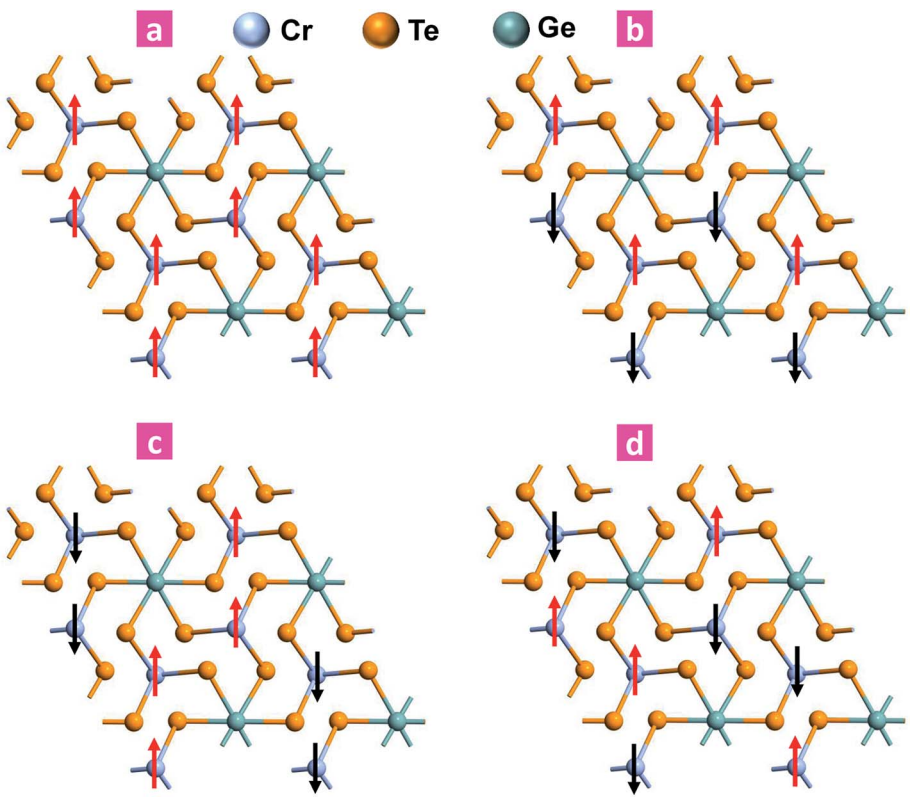

Fig. 1 Schematic representing various magnetic configurations of the CGT in FM and AFM arrangements, namely: (a) FM, (b) AFM1, (c) AFM2, (d) AFM3. The red and black arrows represent the spin-↑ and spin-↓ states respectively.

while spin-↑ being the majority type near the Fermi level (E_F) as shown in Fig. 2a. However, the bandgap starts decreasing on applying tensile strain and it turns metallic at $S_b > 3\%$. This information can also be confirmed from the density of states (DOS) behaviour where the conduction and valence band edges move closer to the Fermi level (E_F) for $S_b = 2\%$ (Fig. 2b). At $S_b = 4\%$, spin-↑ states are present at the Fermi level, while it offers a gap for the spin-↓ states, a signature of half-metallic behaviour as shown in Fig. 2c, which is also noticed in the spin density of states (SDOS) behaviour. Further, it is observed that the system maintains its semiconducting nature in the compressive strain regime with a maximum band gap of 0.5 eV at $S_b = -2\%$, which decreases beyond this value. The variation of bandgap of CGT on applying tensile and compressive strain is depicted in Fig. 2e. Considering the effect of spin orbit coupling (SOC),[39] a direct band gap opening of 0.36 eV is observed for unstrained CGT. The diagrammatic representation of the two band structures (with SOC and without SOC) is provided in Section S5 of the ESI.†[40]

Exfoliation energy is an important parameter to be considered while fabricating 2D structures from their bulk counterparts. In our present work, we have calculated the exfoliation energy of n-layer CGT ($E_{exf}(n)$)[41] and have observed that the energies fall below the range of commonly exfoliated materials, which proves that CGT can be experimentally exfoliated. The detailed information is included in the Section S3 of the ESI.†[40] The stability of the system was studied by analysing the formation energy of CGT as shown in Fig. 2d. The formation energy (E_{form}) was calculated using eqn (1) as,

$$E_{form} = (mE_{Cr} + nE_{Ge} + pE_{Te} - E_{Cr_2Ge_2Te_6})/(m + n + p) \quad (1)$$

where E_{Cr}, E_{Ge} and E_{Te} are the total energies of chromium, germanium and tellurium atoms respectively. $E_{Cr_2Ge_2Te_6}$ is the total energy of a CGT unit cell having $m = n = 2$ and $p = 6$. Using the above equation, the formation energy of unstrained CGT is observed to be 3.7 eV per atom which is comparable to similar 2D systems such as Fe_2Si[42] (4.10 eV per atom) and Ni_2Ge[43] (4.42 eV per atom). The formation energy is reduced with an increase in strain in the tensile as well in the compressive regime, however the variation is not significant, suggesting that the system stays stable under these conditions and similar observation was made in the presence of electric field. In addition, the dynamical stability at high strain and thermal stability of the system at various temperatures is confirmed through phonon dispersion calculations and molecular dynamics (MD) simulations[44] which is elaborated in Section S2 and S4 respectively in the ESI.†[40]

Apart from strain, another way of influencing the electronic properties is through the application of an external electric field. The bandgap decreases from 0.28 eV → 0 eV at $E_z = 0.25$ V Å^{-1} (Fig. 2e). The metallic nature remains upto $E_z = 0.5$ V Å^{-1} as well. However, on further increasing the field to $E_z = 0.75$ V Å^{-1}, a direct band gap opening of 0.19 eV was noticed, which more or less remained the same upto $E_z = 1$ V Å^{-1}. Changing the polarity of the electric field did not disturb this scenario. The electronic and magnetic phase diagram displayed in Fig. 2f and g shows that CGT is semiconducting between the strain range $S_b = -4\%$ to $S_b = 2\%$, while being half-metallic at $S_b = 3\%$ → 4%, $S_b =$

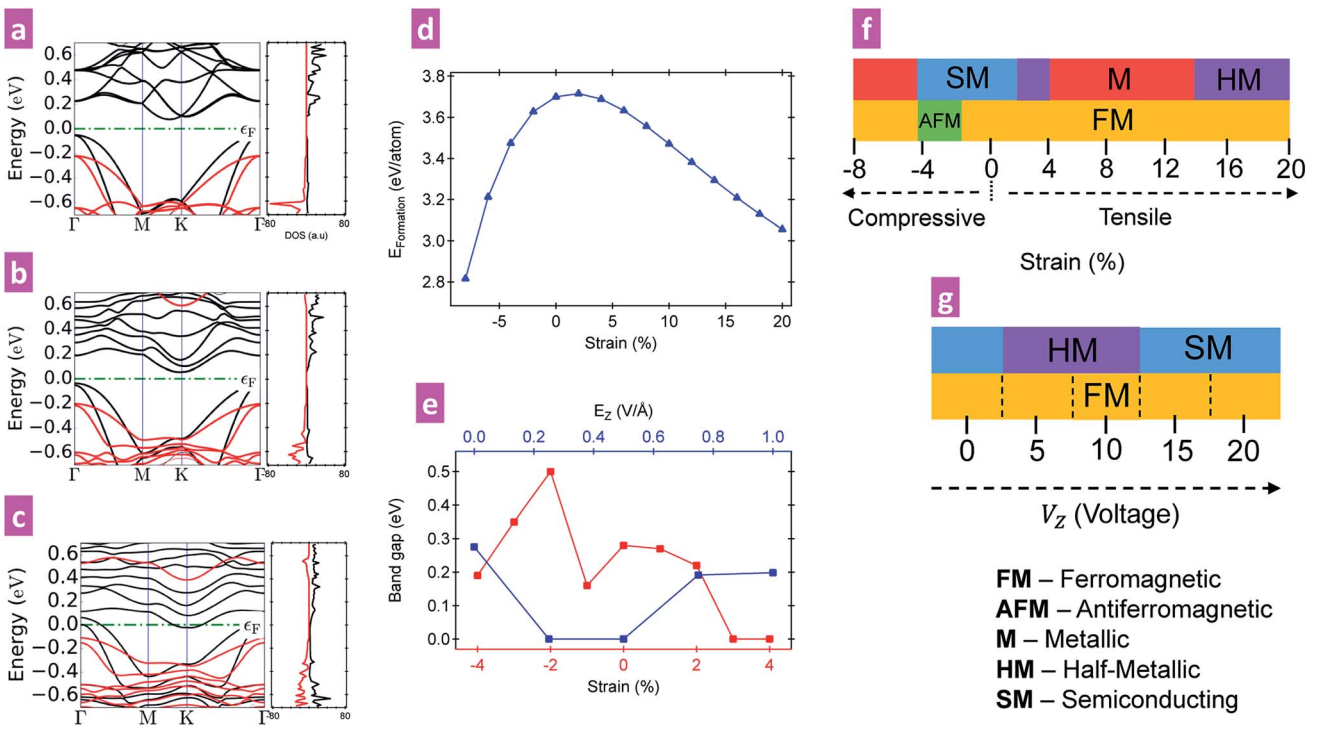

Fig. 2 The bandstructure (left) and spin-polarised density of states (right) for CGT at (a) unstrained, (b) $S_b = 2\%$, (c) $S_b = 4\%$ conditions. The black and red colors represent spin-↑ and spin-↓ contributions respectively. (d) Formation energy of CGT as a function of strain. (e) Strain and electric field dependance of the bandgap. Electronic and magnetic phase diagram of CGT as function of (f) strain ($E_z = 0$) and (g) electric field ($S_b = 0\%$).

14% and beyond this. Metallic region is found between the strain regimes $S_b = -6\% \rightarrow S_b = -8\%$ and $S_b = 5\% \rightarrow S_b = 12\%$. Similarly the phase diagram with electric field applied on unstrained CGT (displayed in Fig. 2f) shows that CGT is half-metallic between $E_z = 0.25$ V Å$^{-1} \rightarrow 0.5$ V Å^{-1}, while remaining semiconducting elsewhere. The system is also observed to be antiferromagnetic for the strain range from $S_b = -2\%$ to $S_b = -4\%$ and stays in the FM state at other values of strain studied in this work. Also the material remains ferromagnetic throughout even on exposing the system to variable electric field. Such a diagram can be very useful in phase designing of the system through strain and electric field tuning.

B Magnetic properties

In order to study the magnetic properties as a function of biaxial strain, we considered all the theoretically possible and distinct magnetic configurations to explore the preferred magnetic ground state exhibited by CGT. The arrangements consisted of one ferromagnetic (i) FM and 3 antiferromagnetic configurations which are named as (ii) AFM1, (iii) AFM2, (iv) AFM3 respectively as portrayed in Fig. 1. The difference between the FM and AFM ground states is expressed in the form of exchange energy calculated using eqn (2) as given below,

$$\Delta E = E_{FM} - E_{AFM} \quad (2)$$

where E_{FM} and E_{AFM} are the energies of the FM and AFM configurations respectively. Here AFM in general corresponds to any of the three (AFM1, AFM2 and AFM3) arrangements depending on the magnetic configuration possessing the lowest energy. The table incorporating the total energies for various magnetic arrangements and energy difference ($E_{FM} - E_{AFM}$), calculated for different strains are provided in Section S1 of the ESI.†[40] ΔE helps in the determination of the type of magnetic ground state, which can be used for the estimation of the critical temperature of the system using the mean field theory. However, this approach generally overestimates the T_c value. Hence to precisely estimate the T_c value, Monte Carlo (MC) simulation based on a two-dimensional (2D) Ising model is used here. This method has been immensely useful for providing the magnetic behaviour of various 2D magnetic system.[45] The interaction between neighbouring spins can be effectively described by the Hamiltonian of 2D Ising model in eqn (3),

$$\mathcal{H} = -\sum_{i>j} J_{ij} S_i \times S_j \quad (3)$$

where J_{ij} is the exchange integral between the spins S_i and S_j located at i^{th} and j^{th} sites and J_{ij} ($=J$) can be estimated from eqn (4) by,

$$J = -\frac{\Delta E}{2S^2} \quad (4)$$

with the S is the value of spin. The system tends to show ferromagnetic ordering when $J > 0$, while antiferromagnetic ordering is observed for $J < 0$. The eqn (3) described above has also been used to estimate the critical temperature of several 2D magnetic materials.[22,42] In the current work, considering the first nearest neighbour interaction of spins is enough to obtain a good agreement of the critical temperature with experimentally obtained value.[46]

The result of a typical MC simulation has been illustrated in Fig. 3 for the unstrained condition. An FM → PM phase transition at a temperature of 61 K can be inferred from the magnetisation curve, which is also well in agreement with the experimentally reported value.[47] The critical temperature can be estimated accurately from the specific heat peak in Fig. 3a as well. The sharp peak in the susceptibility curve in Fig. 3b demonstrates the divergence of the first derivative of the order parameter, characteristics of a 2nd order phase transition. Comparing with the work conducted on similar system, it is observed that in ref. 5, the electronic and magnetic properties of have been reported over a limited strain and electric field range and it does not offer any information on the critical temperature, phase transition *etc.* The results in ref. 4 offers a detailed overview on the magnetic state, critical temperature on the sister compound $Cr_2Ge_2Se_6$ over a strain range upto 7%. The present work offers a unique perspective by combining the effect of strain and electric field on the electronic and magnetic properties of $Cr_2Ge_2Te_6$ over a larger strain range (~20%), which has not been covered before in any of these studies.

Fig. 4a portrays the energy difference between the FM and AFM state for various strain cases along with the strain dependence of T_c in the FM phase. In the unstrained case, negative ΔE

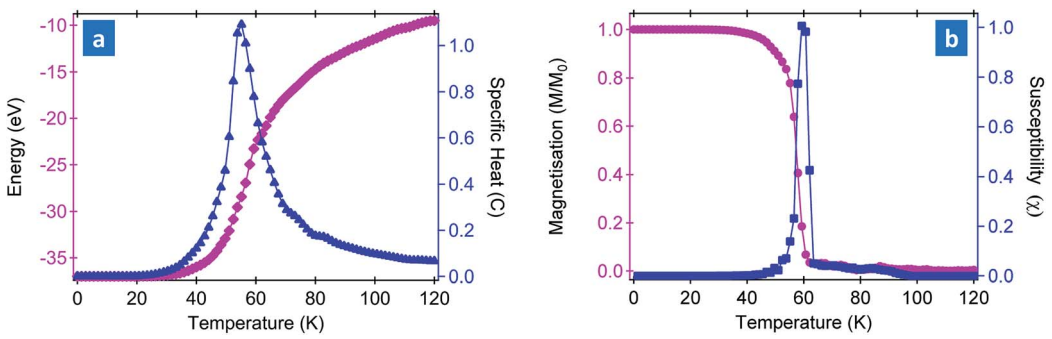

Fig. 3 Temperature dependence of various thermodynamic parameters obtained through Monte Carlo simulations: (a) energy and specific heat, (b) magnetisation and magnetic susceptibility.

indicates CGT to be FM, which agrees with the experimental observation.[32] Under the application of a tensile strain, the T_c gets enhanced rapidly with a maximum of 312 K at $S_b = 8\%$. The rate of enhancement of T_c between unstrained → $S_b = 8\%$ is 32 K/% strain, which shows a significantly high rate of enhancement. However, for strains above $S_b = 10\%$, a gradual drop in T_c is observed with an average rate of reduction ~19 K/% strain from $S_b = 8\%$ → 20%, finally falling to a T_c of 83 K at $S_b =$ 20%. These results indicate the existence of a high degree of FM ordering existing in CGT with a five fold enhancement in the T_c on the application of strain from the unstrained state. Strain dependent studies on $CrXTe_3$ (X = Si, Ge) nanosheets have reported similar enhancement on T_c (35.7 K → 57.2 K for $CrGeTe_3$ and 91.7 K → 108.9 K for $CrSiTe_3$ in the presence of 8% strain).[48] The magnetic moment in CGT is primarily contributed by the Cr-atoms, which in the unstrained case offers a moment ~4.46 μ_B and this value stays of similar order of magnitude over a large strain range. The presence of a room temperature FM ordering through the application of strain and the strain tunability in T_c can facilitate the application of CGT in designing various spin circuits. Magneto-anisotropic energy (MAE) is an important parameter to be considered while analyzing the magntic properties of a system and provides essential information regarding the easy and hard axis of magnetization of materials. For the present case, we have calculated the MAE for different strain percentages of CGT and it was observed that in the unstrained condition, the spins prefer to stay along the in-plane direction. Further information is provided in Section S6 of the ESI.†[40]

The electric field dependence of the T_c is shown in Fig. 4b. In the unstrained case, T_c drops sharply at $E_z > 0$, which does not show significant changes between $E_z = 0.25$ V Å^{-1} → 1 V Å^{-1}. However, in the presence of strain of $S_b = 8\%$, T_c shows interesting variation with the change in E_z. We observed that as the electric field increases there is a gradual decrease in T_c, with a value of 303 K at $E_z = 0.25$ V Å^{-1}. However, with further increment in E_z, T_c increases monotonically reaching a value of 331 K for an applied field of $E_z = 1$ V Å^{-1}. The T_c value is higher than the maximum T_c estimated only in the presence of strain, with 5.5 times higher than the value from the pristine configuration, suggesting the association of electric field and strain offers superior enhancement of T_c and the FM properties in CGT. It was also observed that swapping the direction of electric field also offers a similar T_c behaviour. The massive escalation in T_c through coupling strain with electric field is a note-worthy mechanism for enhancing the ferromagnetic ordering temperature, which is by far an unexplored option to the best of our knowledge. The electric field effect on the material is understood by analysing the projected density of states (PDOS) of the system. Details regarding the same are included in Section S7 of the ESI.†[40]

The existence of a sustainable magnetic ordering in CGT is facilitated through the exchange interaction between the Cr atoms, mediated *via* tellurium atoms as seen from the electron density iso-surface plot in Fig. 5a. The viable path for indirect exchange is through Te–Cr–Te bonds and the projected density of states (PDOS) analysis revealed that the $d_{xz}/d_{x^2-y^2}$ orbitals of Cr and p_z/p_x orbitals of Te contribute primarily towards this as observed from Fig. 5b. Furthermore, it could be seen that as the strain is increased the orbital contributions from the Te atoms increases dramatically near the Fermi level, owing to the high T_c observed at $S_b = 8\%$ as displayed in Fig. 5c. The degree of orbital overlap determines the strength of exchange interaction (J) which further promotes an increase in T_c. The extent of the overlap is maximum at $S_b = 8\%$ and further overlap extension breaks down as we go beyond 8% strain, which then results in the decrease of T_c. There was a decrease in T_c observed when unstrained CGT was exposed to electric field. The reason for this also lies in the superexchange between the Cr atoms *via* Te atom. There is a drastic decrease in the density of states of the p_z and p_x orbitals of Te on the application of electric field. However strained ($S_b = 8\%$) CGT on interaction with electric field showed an escalation in critical temperature. In this scenario there is an increase in the DOS of all the components of p-orbitals (p_z, p_x, p_y) of Te atoms at the Fermi level which is responsible for the enhancement of T_c.

Superexchange is basically an indirect exchange mechanism occurring in ionic solids since there is no direct overlap between the magnetic metal atoms (Cr atoms in our case). It is mediated *via* a non-magnetic atom (Te atom in this case) which is placed between the two magnetic ions. This indirect exchange allows in lowering of the kinetic energy of the system by allowing the unpaired electrons on the metal atoms to be easily delocalized over the whole structure through the non-magnetic atom. It is a second order process and is derived from the second-order perturbation

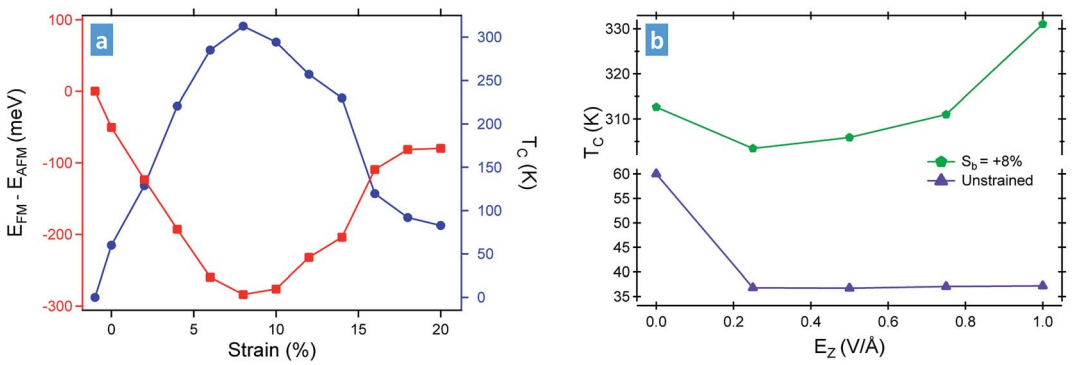

Fig. 4 (a) Strain dependance of the energy difference ($E_{FM} - E_{AFM}$) and the critical temperature, (b) T_c as function of E_z in the unstrained (bottom panel) and strained ($S_b = 8\%$) configuration (top panel).

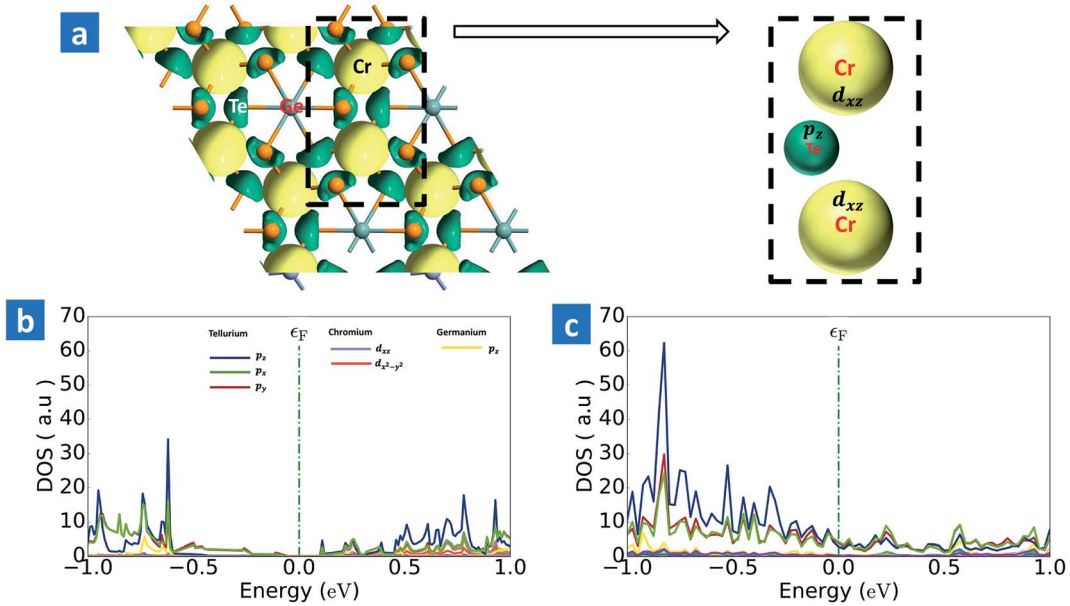

Fig. 5 (a) Spin-electron difference density iso-surface of $Cr_2Ge_2Te_6$ in the unstrained condition with a iso-value of 0.05 $Å^{-3}$. The projected density of states (PDOS) of CGT at (b) unstrained and (c) $S_b = 8\%$ configuration.

theory. From a mechanical point of view, the angle of the Cr–Te–Cr bond changes in the presence of strain, which as per Goodenough–Kanamori rule[49,50] can lead to a varied degree of ferromagnetism as the bond angle deviates from 180°. Under such circumstance, the antiferromagnetic coupling between the Cr and Te atoms stays proportional to $(\sim t^2/\delta\varepsilon)$, where t is the hopping term between Te-4p and Cr-3d orbitals and $\delta\varepsilon$ is the energy difference between them.[4] While it was observed that t stays of similar value, $\delta\varepsilon$ gets reduced in the presence of strain. This leads to an enhancement of the AFM coupling between Cr and Te atoms, strengthening the FM coupling between Cr atoms involved in the superexchange path of Cr–Te–Cr. This explains the enhancement of the T_c upto $S_b = 8\%$. The present study involves exposing the material to a variety of excitation, like a large value of strain and electric field and the material is found to be stable under such conditions. In an experimental situation, pre-stretched substrates can be used for applying strain on a 2D material or special substrates with 3D-nanostructure can be prepared upon which a 2D material can be transferred. Upon restoration of such substrates from flat condition, relatively high value of strain could be achieved. Other possible systems where high compressive strain could be expected is when one 2D layer edge is anchored, and locally a scanning microscopy probe tip is used to compress the system. The present results offers direction for tuning the magnetic phase as well T_c of a 2D magnetic system without causing permanent changes to the structure, which can have immense importance for future spintronics device development.

IV Conclusion

We have investigated the influence of strain and electric field on the electronic and magnetic behaviour of a novel 2D magnetic material $Cr_2Ge_2Te_6$ through first-principles based calculations. Under the influence of biaxial strain, the material goes through a semiconductor → half-metallic phase and FM → AFM transition as well as rapid changes in the T_c, suggesting the existence of a high temperature ferromagnetic ordering which is unique in such 2D materials. The origin of such behaviour lies in the strength of overlap between various orbitals of Cr mediated *via* the Te atom in the superexchange process across Cr–Te–Cr path. Further enhancement in T_c is possible when the material is exposed to electric field, leading to a $T_c \sim 331$ K, nearly 6 times from the initial unstrained condition. Our current approach offers a novel route of engineering the electronic and magnetic properties of a 2D material in a non-destructive manner which is essential for future magneto-electronic and spintronic device applications.

Conflicts of interest

There are no conflicts to declare.

Acknowledgements

This work was financially supported by the Department of Science and Technology, India through the INSPIRE scheme (Ref: DST/INSPIRE/04/2015/003087), ECR Grant (Ref: ECR/2017/002223) and CRG Grant (Ref: CRG/2019/003289). SJR sincerely acknowledges the support provided by UGC-DAE Consortium for Scientific Research (Ref: CSR-IC-263 and CRS-M-321) and Indian Institute of Technology Patna.

References

1 A. Chaudhury, S. Majumder and S. J. Ray, *Phys. Rev. Appl.*, 2019, **11**, 024056.
2 M. Sun, Y. Hao, Q. Ren, Y. Zhao, Y. Du and W. Tang, *Solid State Commun.*, 2016, **242**, 36–40.

3 A. K. Nair, P. Kumari, M. Venkata Kamalakar and S. J. Ray, *Phys. Chem. Chem. Phys.*, 2019, **21**, 23713–23719.
4 X.-J. Dong, J.-Y. You, B. Gu and G. Su, *Phys. Rev. Appl.*, 2019, **12**, 014020.
5 K. Wang, T. Hu, F. Jia, G. Zhao, Y. Liu, I. V. Solovyev, A. P. Pyatakov, A. K. Zvezdin and W. Ren, *Appl. Phys. Lett.*, 2019, **114**, 092405.
6 S. J. Ray and M. Venkata Kamalakar, *Phys. Chem. Chem. Phys.*, 2018, **20**, 13508–13516.
7 P. Srivastava, K. Hembram, H. Mizuseki, K.-R. Lee, S. S. Han and S. Kim, *J. Phys. Chem. C*, 2015, **119**, 6530–6538.
8 Y. Liu, C. Xiao, Z. Li and Y. Xie, *Adv. Energy Mater.*, 2016, **6**, 1600436.
9 S. Rani and S. J. Ray, *Phys. Chem. Chem. Phys.*, 2020, **22**, 11452–11459.
10 S. Zhang, N. Wang, S. Liu, S. Huang, W. Zhou, B. Cai, M. Xie, Q. Yang, X. Chen and H. Zeng, *Nanotechnology*, 2016, **27**, 274001.
11 S. Rani and S. J. Ray, *Carbon*, 2019, **144**, 235–240.
12 S. Rani and S. J. Ray, *Carbon*, 2020, **173**, 493–500.
13 J. F. Dayen, S. J. Ray, O. Karis, I. J. Vera-Marun and M. V. Kamalakar, *Appl. Phys. Rev.*, 2020, **7**, 011303.
14 P. Kumari, S. Majumder, S. Rani, A. K. Nair, K. Kumari, M. Venkata Kamalakar and S. J. Ray, *Phys. Chem. Chem. Phys.*, 2020, **22**, 5893–5901.
15 L. Onsager, *Phys. Rev.*, 1944, **65**, 117–149.
16 N. D. Mermin and H. Wagner, *Phys. Rev. Lett.*, 1966, **17**, 1133–1136.
17 P. C. Hohenberg, *Phys. Rev.*, 1967, **158**, 383.
18 B. Huang, G. Clark, E. Navarro-Moratalla, D. R. Klein, R. Cheng, K. L. Seyler, D. Zhong, E. Schmidgall, M. A. McGuire, D. H. Cobden, W. Yao, D. Xiao, P. Jarillo-Herrero and X. Xu, *Nature*, 2017, **546**, 270–273.
19 J.-U. Lee, S. Lee, J. H. Ryoo, S. Kang, T. Y. Kim, P. Kim, C.-H. Park, J.-G. Park and H. Cheong, *Nano Lett.*, 2016, **16**, 7433–7438.
20 V. Carteaux, D. Brunet, G. Ouvrard and G. Andre, *J. Phys.: Condens. Matter*, 1995, **7**, 69.
21 M. Bonilla, S. Kolekar, Y. Ma, H. C. Diaz, V. Kalappattil, R. Das, T. Eggers, H. R. Gutierrez, M.-H. Phan and M. Batzill, *Nat. Nanotechnol.*, 2018, **13**, 289–293.
22 A. K. Nair, S. Rani, M. Venkata Kamalakar and S. J. Ray, *Phys. Chem. Chem. Phys.*, 2020, **22**, 12806–12813.
23 S. Rani, A. K. Nair, M. Venkata Kamalakar and S. J. Ray, *J. Phys.: Condens. Matter*, 2020, **32**, 415301.
24 W. Xing, Y. Chen, P. M. Odenthal, X. Zhang, W. Yuan, T. Su, Q. Song, T. Wang, J. Zhong, S. Jia, *et al.*, *2D Materials*, 2017, **4**, 024009.
25 Y. Liu and C. Petrovic, *Phys. Rev. B*, 2018, **97**, 014420.
26 J. Zhang, B. Zhao, Y. Yao and Z. Yang, *Phys. Rev. B: Condens. Matter Mater. Phys.*, 2015, **92**, 165418.
27 C. Xu, J. Feng, H. Xiang and L. Bellaiche, *npj Comput. Mater.*, 2018, **4**, 1–6.
28 L. Alegria, H. Ji, N. Yao, J. Clarke, R. J. Cava and J. R. Petta, *Appl. Phys. Lett.*, 2014, **105**, 053512.
29 M. Mogi, A. Tsukazaki, Y. Kaneko, R. Yoshimi, K. S. Takahashi, M. Kawasaki and Y. Tokura, *APL Mater.*, 2018, **6**, 091104.
30 Y. Fang, S. Wu, Z. Z. Zhu and G. Y. Guo, *Phys. Rev. B*, 2018, **98**, 125416.
31 K. L. Seyler, D. Zhong, D. R. Klein, S. Gao, X. Zhang, B. Huang, E. Navarro-Moratalla, L. Yang, D. H. Cobden, M. A. McGuire and W. Yao, *Nat. Phys.*, 2018, **14**, 277–281.
32 C. Gong, L. Li, Z. Li, H. Ji, A. Stern, Y. Xia, T. Cao, W. Bao, C. Wang, Y. Wang, *et al.*, *Nature*, 2017, **546**, 265–269.
33 S. Smidstrup, T. Markussen, P. Vancraeyveld, J. Wellendorff, J. Schneider, T. Gunst, B. Verstichel, D. Stradi, P. A. Khomyakov, U. G. Vej-Hansen and M. E. Lee, *J. Phys.: Condens. Matter*, 2019, **32**, 015901.
34 P. Giannozzi, S. Baroni, N. Bonini, M. Calandra, R. Car, C. Cavazzoni, D. Ceresoli, G. L. Chiarotti, M. Cococcioni, I. Dabo and A. Dal Corso, *J. Phys.: Condens. Matter*, 2009, **21**, 395502.
35 J. P. Perdew, K. Burke and M. Ernzerhof, *Phys. Rev. Lett.*, 1996, **77**, 3865.
36 H. J. Monkhorst and J. D. Pack, *Phys. Rev. B: Solid State*, 1976, **13**, 5188–5192.
37 S. Grimme, *J. Comput. Chem.*, 2006, **27**, 1787–1799; S. Grimme, J. Antony, S. Ehrlich and H. Krieg, *J. Chem. Phys.*, 2010, **132**, 154104.
38 J. V. Selinger, *Introduction to the theory of soft matter: from ideal gases to liquid crystals*, Springer, 2015.
39 C. He, M. Cheng and W. X. Zhang, *Mater. Res. Express*, 2018, **5**, 065059.
40 A. K. Nair, *et al.*, See ESI† for additional results on electronic phase-crossover and room temperature ferromagnetism in a two-dimensional (2D) spin lattice.
41 T. Li, C. He and W. Zhang, *Energy Storage Mater.*, 2020, **25**, 866–875.
42 Y. Sun, Z. Zhuo, X. Wu and J. Yang, *Nano Lett.*, 2017, **17**, 2771–2777.
43 L-M. Yang, I. A. Popov, T. Frauenheim, A. I. Boldyrev, T. Heine, V. Bacic and E. Ganz, *Phys. Chem. Chem. Phys.*, 2015, **17**, 26043–26048.
44 C. He, M. Zhang, T. T. Li and W. X. Zhang, *J. Mater. Chem. C*, 2020, **8**, 6542–6551.
45 M.-W. Lin, H. L. Zhuang, J. Yan, T. Z. Ward, A. A. Puretzky, C. M. Rouleau, Z. Gai, L. Liang, V. Meunier, B. G. Sumpter, *et al.*, *J. Mater. Chem. C*, 2016, **4**, 315–322.
46 N. Sivadas, M. W. Daniels, R. H. Swendsen, S. Okamoto and D. Xiao, *Phys. Rev. B: Condens. Matter Mater. Phys.*, 2015, **91**, 235425.
47 M. Lohmann, T. Su, B. Niu, Y. Hou, M. Alghamdi, M. Aldosary, W. Xing, J. Zhong, S. Jia, W. Han, *et al.*, *Nano Lett.*, 2019, **19**, 2397–2403.
48 X. Li and J. Yang, *J. Mater. Chem. C*, 2014, **2**, 7071–7076.
49 J. B. Goodenough, *Phys. Rev.*, 1955, **100**, 564.
50 J. Kanamori, *J. Appl. Phys.*, 1960, **31**, S14–S23.